Search for Daily Modulation of MeV Dark Matter Signals with DAMIC-M

I. Arnquist,[1] N. Avalos,[2] D. Baxter,[3,*] X. Bertou,[2] N. Castelló-Mor,[4] A. E. Chavarria,[5] J. Cuevas-Zepeda,[3] A. Dastgheibi-Fard,[6] C. De Dominicis,[7] O. Deligny,[8] J. Duarte-Campderros,[4] E. Estrada,[2] N. Gadola,[9] R. Gaïor,[7] T. Hossbach,[1] L. Iddir,[7] B. J. Kavanagh,[4] B. Kilminster,[9] A. Lantero-Barreda,[4] I. Lawson,[10] S. Lee,[9] A. Letessier-Selvon,[7] P. Loaiza,[8] A. Lopez-Virto,[4] K. J. McGuire,[5] P. Mitra,[5] S. Munagavalasa,[3] D. Norcini,[3,11] S. Paul,[3] A. Piers,[5] P. Privitera,[3,7] P. Robmann,[9] S. Scorza,[6] M. Settimo,[12] R. Smida,[3] M. Traina,[5,7] R. Vilar,[4] G. Warot,[6] R. Yajur,[3] and J-P. Zopounidis[7]

(DAMIC-M Collaboration)

[1]*Pacific Northwest National Laboratory (PNNL), Richland, Washington, USA*
[2]*Centro Atómico Bariloche and Instituto Balseiro, Comisión Nacional de Energía Atómica (CNEA), Consejo Nacional de Investigaciones Científicas y Técnicas (CONICET), Universidad Nacional de Cuyo (UNCUYO), San Carlos de Bariloche, Argentina*
[3]*Kavli Institute for Cosmological Physics and The Enrico Fermi Institute, The University of Chicago, Chicago, Illinois, USA*
[4]*Instituto de Física de Cantabria (IFCA), CSIC—Universidad de Cantabria, Santander, Spain*
[5]*Center for Experimental Nuclear Physics and Astrophysics, University of Washington, Seattle, Washington, USA*
[6]*LPSC LSM, CNRS/IN2P3, Université Grenoble-Alpes, Grenoble, France*
[7]*Laboratoire de physique nucléaire et des hautes énergies (LPNHE), Sorbonne Université, Université Paris Cité, CNRS/IN2P3, Paris, France*
[8]*CNRS/IN2P3, IJCLab, Université Paris-Saclay, Orsay, France*
[9]*Universität Zürich Physik Institut, Zürich, Switzerland*
[10]*SNOLAB, Lively, Ontario, Canada*
[11]*Department of Physics and Astronomy, Johns Hopkins University, Baltimore, Maryland, USA*
[12]*SUBATECH, Nantes Université, IMT Atlantique, CNRS/IN2P3, Nantes, France*

(Received 17 July 2023; revised 7 November 2023; accepted 7 February 2024; published 7 March 2024)

Dark matter (DM) particles with sufficiently large cross sections may scatter as they travel through Earth's bulk. The corresponding changes in the DM flux give rise to a characteristic daily modulation signal in detectors sensitive to DM-electron interactions. Here, we report results obtained from the first underground operation of the DAMIC-M prototype detector searching for such a signal from DM with MeV-scale mass. A model-independent analysis finds no modulation in the rate of 1 e^- events with sidereal period, where a DM signal would appear. We then use these data to place exclusion limits on DM in the mass range $[0.53, 2.7]$ MeV$/c^2$ interacting with electrons via a dark photon mediator. Taking advantage of the time-dependent signal we improve by ~2 orders of magnitude on our previous limit obtained from the total rate of 1 e^- events, using the same dataset. This daily modulation search represents the current strongest limit on DM-electron scattering via ultralight mediators for DM masses around 1 MeV$/c^2$.

DOI: 10.1103/PhysRevLett.132.101006

Introduction.—There are numerous astrophysical and cosmological observations supporting the existence of a nonbaryonic and nonluminous form of matter [1], known as dark matter (DM). Despite a wealth of experimental efforts to detect DM through its nongravitational interactions [2–4], its identity remains unknown. DM particles with MeV-scale masses are viable candidates that appear in a range of natural, well-motivated scenarios [5–9]. However, their discovery remains challenging since such light particles do not have sufficient kinetic energy to produce detectable nuclear recoils in direct-detection experiments [10]. Instead, *DM-electron* scattering would produce eV-scale electronic recoils, which would be observed in semiconductor-based detectors with $\mathcal{O}(1\ \mathrm{eV})$ ionization thresholds [11]. To date, the sensitivity of semiconductor searches [12–16] has been partly limited by background levels [17]. A time-dependent DM signal detected above a time-independent background can significantly increase the sensitivity of these searches.

Various phenomena give rise to a daily modulation in the flux of DM, including the variation of the velocity of

the lab frame due to Earth's rotation [18] and gravitational focusing of the DM flux by Earth [18–20]. Furthermore, if the DM scattering cross section is sufficiently large, the velocity distribution of DM particles at the detector may be distorted by their interactions in Earth [21–23]. Over the course of a sidereal day, the position of the detector rotates with respect to the incoming DM flux. Thus, the DM particles will travel a greater or smaller distance across Earth at different times, leading to a daily modulation.

Most experimental searches for daily modulations [24–27] have targeted DM particles interacting with nuclei. Here, we focus on models with MeV-scale DM, which may be coupled to standard model particles via a kinetically mixed dark photon [28,29], and thus interact with electrons. For DM-electron scattering cross sections currently within reach of semiconductor searches, interactions in Earth may be substantial [30], which motivate the search for a daily modulated signal on top of a constant background [31,32].

In this Letter, we present a search for a daily modulated signal with a prototype of the DAMIC-M (Dark Matter in CCDs at Modane) experiment [33]. We first perform a model-independent search for modulations over a wide range of periods. We then report limits on DM particles with MeV-scale masses interacting with electrons, which incorporate, for the first time with an underground detector, a time-dependent analysis to provide a powerful discriminant between signal and background.

Setup and data.—The DAMIC-M experiment will feature ~200 skipper charge-coupled devices (CCDs), for a target silicon mass of ~700 g, installed under the French Alps at the Laboratoire Souterrain de Modane (LSM). DAMIC-M is sensitive to a single-ionization charge signal thanks to the extremely low level of dark current and the subelectron readout noise of the devices. By operating prototype CCDs at LSM in the Low Background Chamber (LBC) we obtained world-leading limits on sub-GeV DM particles interacting with electrons [16]. The daily modulation results reported here are obtained with the same apparatus and dataset, which are summarized in the following.

Two high-resistivity ($>10\ \mathrm{k\Omega\,cm}$), n-type silicon CCDs [34–36] are installed in the LBC. Each CCD has 6144×4128 pixels (pixel area $15 \times 15\ \mu\mathrm{m}^2$) and is 670 μm thick, for a mass of ~9 g. The detectors are mounted in a high-purity copper box, which also shields infrared radiation. A lead shield of ~7.5 cm thickness, with the innermost 2 cm of ancient origin [37], encloses the copper box inside the LBC cryostat. An additional 15 cm of lead and 20 cm of high density polyethylene surround the cryostat to shield from environmental radiation. The measured background between 1 and 20 keV is $\sim 10\ \mathrm{events\,keV^{-1}\,kg^{-1}\,day^{-1}}$, consistent with expectations from a GEANT4 [38] Monte Carlo simulation of the apparatus. The CCDs are kept at a temperature of ~130 K inside the vacuum cryostat at $\sim 5 \times 10^{-6}$ mbar.

Charge carriers produced by ionizing radiation in the silicon bulk of the CCD drift toward the x-y plane where pixels are located. Thermal diffusion while drifting results in a spatial variance σ_{xy}^2 of the charge collected in contiguous pixels [39]. In the readout process, the pixel charge is moved across the array by appropriate voltage clocking and read out serially by two amplifiers (referred to as U and L) located at the corners of the CCD at the end of the serial register. These skipper amplifiers [40–42] allow for multiple nondestructive measurements (NDCMs) of the pixel charge. Subelectron resolution is achieved by averaging a sufficient number (N_{skips}) of NDCMs, with the resolution improving as $1/\sqrt{N_{\mathrm{skips}}}$. The performance of DAMIC-M CCDs is detailed in Ref. [43].

For this analysis we use 63 days of uninterrupted data taking beginning on June 8, 2022 (the SR2 dataset in Ref. [16]). Relevant CCD operating parameters include $N_{\mathrm{skips}} = 650$, corresponding to a pixel charge resolution of $\sim 0.2e^-$, and a 10×10 pixel binning. In subsequent text, the term pixel is used to describe a 10×10 bin of pixels from which charge is summed before being read out. To minimize dark current counts, only a fraction of the CCD is read out (640×110 pixels), and its charge is cleared between consecutive images.

Image data reduction and pixel selection criteria are detailed in Ref. [16]. In brief, images are first calibrated from the fitted position of the $0e^-$ and $1e^-$ peaks in the pixel charge distribution. Then contiguous pixels with charge are joined into clusters. Those with total charge $>7e^-$ are excluded from further analysis since they are unlikely to be produced by sub-GeV DM interactions with electrons. For each cluster we also exclude 10 trailing pixels in the horizontal and vertical directions to account for charge transfer inefficiencies. Defects in the CCDs may release charge during the readout, appearing in the images as "hot" pixels and columns [44]. These are identified by their increased rate of pixels with $1e^-$, and rejected. Lastly, we exclude one of the prototype CCDs due to the presence of several charge traps in the serial register (identified by a decreased rate of pixels with $1e^-$). A portion of the remaining CCD is also excluded for the same reason. The final integrated exposure after applying these selection criteria is 39.97 g days, distributed over $N_{\mathrm{im}} = 8779$ images.

For each image i the charge distribution of the selected pixels is fitted with the sum of two Gaussian functions corresponding to the $0e^-$ and $1e^-$ peaks. The number of pixels with $1e^-$ charge, N_1^i, and its uncertainty $\sigma_{N_1}^i$ are then obtained from the fitted parameters. The U and L sides of the image are fitted independently to account for small differences in the calibration and resolution of the amplifiers. We find the value of N_1^i to be ~80 and ~30 pixels/image for the U and L amplifier, respectively. The difference in counts is due to a large portion of the L side being excluded by the serial register trap criteria. Corresponding rates of $1e^-$, R_1^i, and associated uncertainties $\sigma_{R_1}^i$ are then

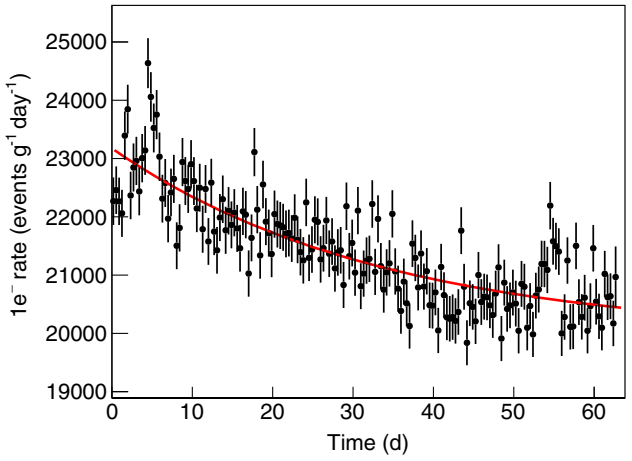

FIG. 1. Measured rate of $1e^-$, R_1^i, as a function of time for the U side. Each data point is the rate averaged over 50 images. The red line is the result of the fit of a constant plus an exponential.

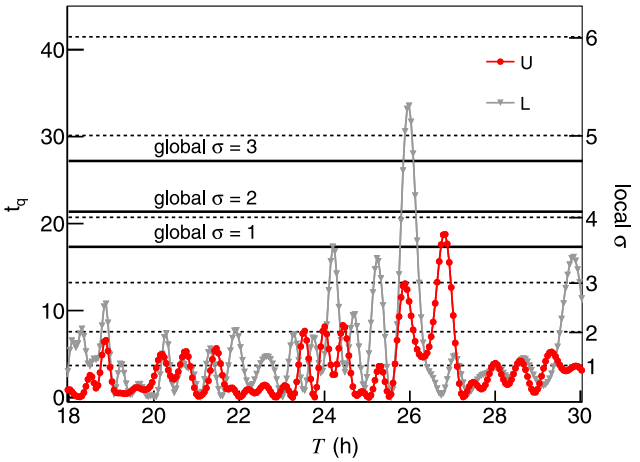

FIG. 2. Model-independent search for daily modulation. The test statistic t_q and corresponding local significance as a function of the modulation period T in a range around 24 h; the global significance levels for 1σ, 2σ, and 3σ are also shown as horizontal lines. Both local and global significances are one-sided. See text for details.

obtained dividing N_1^i and $\sigma_{N_1}^i$ by the effective image exposure time ($t_{\rm exp} = 0.003\,56$ days) and target mass after pixel selection. For each image the relative uncertainty $\sigma_{R_1}^i/R_1^i$ is ∼13% (21%) for the U (L) side. This set of $1e^-$ rates, measured every ∼10 min for 63 consecutive days, is used to search for a daily modulation.

The rate R_1^i for the U side is shown as a function of time in Fig. 1. The rate is well parametrized by a constant plus an exponential with time decay constant $\tau \sim 33.5$ days. The L side has the same behavior. Since $\tau \gg 1$ day, a daily modulation analysis is largely unaffected. The observed time dependence is consistent with the dark current stabilizing over time, a characteristic of these types of devices [44].

Model-independent search for a daily modulation.—We first perform a model-independent analysis by fitting the measured rates R_1^i to a function $F(t) = Be^{-t/\tau} + C + A\cos[(2\pi(t-\phi)/T]$, where B, C, and τ parametrize the exponential time dependence observed in the data, and A, T, and ϕ are the modulation amplitude, period, and phase. This simplified model approximates a periodic signal with the first term of its Fourier expansion. We use a binned likelihood method to test the null hypothesis, i.e., absence of modulation, corresponding to $A = 0$. The likelihood function is

$$\mathcal{L}(\theta) = \prod_{i=1}^{N_{\rm im}} \frac{1}{\sqrt{2\pi}\sigma_{R_1}^i} \exp\left\{-\frac{1}{2}\left(\frac{R_1^i - F(t_i|\theta)}{\sigma_{R_1}^i}\right)^2\right\}, \quad (1)$$

where $\theta = \{A, B, C, \tau, T, \phi\}$ is the set of model parameters and t_i is the time [45] when image i was taken. The spread in the arrival time of the events within each image has negligible impact for the range of periods explored. The likelihood of the no-modulation hypothesis H_0 is found by maximizing Eq. (1) under the constraint $A = 0$, $\mathcal{L}_{H_0} = \sup_{A=0}\mathcal{L}(\theta)$, while the global maximum for a given period T is $\mathcal{L}_{H_1} = \sup_\theta \mathcal{L}(\theta)$. The likelihood-ratio test statistic for the H_0 hypothesis is given by $t_q = -2\ln(\mathcal{L}_{H_0}/\mathcal{L}_{H_1})$. The local significance of a departure from the H_0 hypothesis for any given period T can then be quantified by the value of t_q [46]. In Fig. 2 we show the value of the test statistic and the corresponding local and global significance as a function of T in a range around 24 h. Global significances are calculated by examining the distribution of the maximum value of the test statistic under H_0 [47], accounting for the search range $T = 1$–48 h. The measured rate is consistent with the null hypothesis (no modulation) for the sidereal period ($T = 23.93$ h), where a DM signal would appear. The same conclusion is drawn for all other periods in the search range, with the only deviation found for $T = 26$ h in the L side. This deviation has no effect on the DM-e^- scattering search (see Supplemental Material for details [48]).

DM-e^- scattering.—In this section, we introduce a new approach for constraining DM-e^- scattering, which exploits the expected daily modulation due to DM interactions within Earth. The rate of DM-e^- scattering in a semiconductor is obtained by convolving the scattering cross section with the DM velocity distribution at the detector $f(\mathbf{v}, t)$ and with the crystal form factor $f_{\rm c}$ [11,56,57]:

$$\frac{{\rm d}R}{{\rm d}E_e} \propto \bar{\sigma}_e \int \frac{{\rm d}q}{q^2}\left[\int \frac{f(\mathbf{v},t)}{v}{\rm d}^3v\right]|F_{\rm DM}(q)|^2|f_{\rm c}(q,E_e)|^2. \quad (2)$$

Here, $\bar{\sigma}_e$ is a reference DM-e^- scattering cross section, E_e is the energy deposited as ionization, and q is the momentum transfer. We consider a model of DM which couples to standard model particles via a kinetically mixed

dark photon. In this case, the DM form factor $F_{\rm DM} = (\alpha m_e/q)^n$ depends on the mass of the mediator $m_{A'}$, with $n = 0$ for a heavy mediator ($m_{A'} \gg \alpha m_e$) and $n = 2$ for ultralight mediators ($m_{A'} \ll \alpha m_e$) [30].

The velocity distribution of DM is expected to follow a Maxwell-Boltzmann distribution in the Galactic frame [58,59]. The velocity distribution at the detector is obtained by boosting into the rest frame of the laboratory, which is moving at a velocity $\mathbf{v}_{\rm lab}(t) = \mathbf{v}_\odot + \mathbf{v}_{\rm E}(t) + \mathbf{v}_{\rm rot}(t)$. Here, $\mathbf{v}_\odot$ is the velocity of the Sun in the Galactic frame, $\mathbf{v}_{\rm E}(t)$ Earth's velocity in the Solar frame [61], and $\mathbf{v}_{\rm rot}(t)$ is the rotational velocity of the lab in an Earth-centered inertial frame (see Ref. [62], Appendix A). The velocity distribution $f(\mathbf{v}, t)$ at the detector is therefore always time dependent due to Earth's motion.

If the DM-scattering cross section is sufficiently large, however, the flux of DM may also be distorted by scattering of particles in Earth before they reach the detector. The velocity distribution then depends on the isodetection angle Θ [62], defined as the angle between the local zenith and the direction of the mean DM flux $\langle \mathbf{v}_\chi \rangle = -\mathbf{v}_{\rm lab}$. For $\Theta = 0°$, the mean DM flux comes from directly above the detector, while at $\Theta = 180°$, it comes from directly below. The isodetection angle oscillates over a sidereal day with Earth's rotation, and thus the expected DM flux. During the data-taking period the isodetection angle at LSM (45.2 °N) varied in the range $\Theta \in [0°, 92°]$.

Depending on the regime of interest, a number of formalisms have been developed to estimate the DM flux at the detector as a function of Θ, taking into account Earth scattering (e.g., [31,62–67]). Here, we employ a modified version of the VERNE code [68–70], which assumes that light DM particles travel along straight-line trajectories and either continue unaffected or are reflected back along their incoming path when they scatter [71]. DM scattering with Earth nuclei, implemented in VERNE with charge screening [30], is the dominant process for daily modulation effects. Since each t_i corresponds to a $\Theta(t_i)$ [72], this code allows us to efficiently calculate $f(\mathbf{v}, t_i)$ over a wide range of parameter space.

We search for a daily modulation of the rate R_1^i by performing a likelihood fit with Eq. (1), where F includes both the background and signal model. For the background we use a Poisson model, $P(n_q|\lambda)$, which gives the probability of measuring n_q charges in a pixel given a dark current λ (in units of counts/image). As shown in Fig. 1, the dark current in our data stabilizes with an exponential decrease in time. Thus, we model the time-dependent dark current as $\lambda(t_i) = \lambda_A \exp(-t_i/\tau) + \lambda_{\rm eq}$, where λ_A and τ are the amplitude and time constant of the exponential decay of the dark current, and $\lambda_{\rm eq}$ is its value once stabilized. The signal model, $S(n_q|m_\chi, \bar{\sigma}_e, t_i)$, gives the probability that n_q charges are measured in a pixel for DM particles of mass m_χ and cross section $\bar{\sigma}_e$; the time dependence in S accounts for the expected daily modulation. The fitting function in Eq. (1) is then

$$F(t_i|\theta) = \frac{1}{t_{\rm exp} m_{\rm pix}} \sum_{j=0}^{1} P[1 - j|\lambda(t_i)] S(j|m_\chi, \bar{\sigma}_e, t_i), \qquad (3)$$

where $m_{\rm pix}$ is the mass of one CCD pixel and $\theta = \{\lambda_A, \tau, \lambda_{\rm eq}, \bar{\sigma}_e\}$ are free parameters in the fit. The signal model S is derived with the following procedure. First, the rate as a function of the energy E_e deposited in the DM interaction is computed with Eq. (2) using QEDark [11] for the crystal form factor f_c, which encodes the electronic response of the target. Then, E_e is converted to electron-hole pairs with a semiempirical model based on probabilities $P_{\rm pair}(n_q|E_e)$ from the charge yield model in Ref. [73]. To include the detector response, we perform a Monte Carlo simulation of the charge diffusion process, with σ_{xy}^2 obtained from a surface laboratory calibration with cosmic rays [16,74]. Lastly, a 10×10 binning of the simulated pixel array is applied to match the data-taking conditions.

We minimize the joint log-likelihood for the U and L sides at fixed DM masses between 0.53 and 2.7 MeV/c^2. To illustrate the sensitivity of the method, we show in Fig. 3 the residual rate after background subtraction, obtained by fitting the U-side data to the background model only. Also shown is the expectation for a DM particle of mass 1 MeV/c^2 interacting via an ultralight mediator with

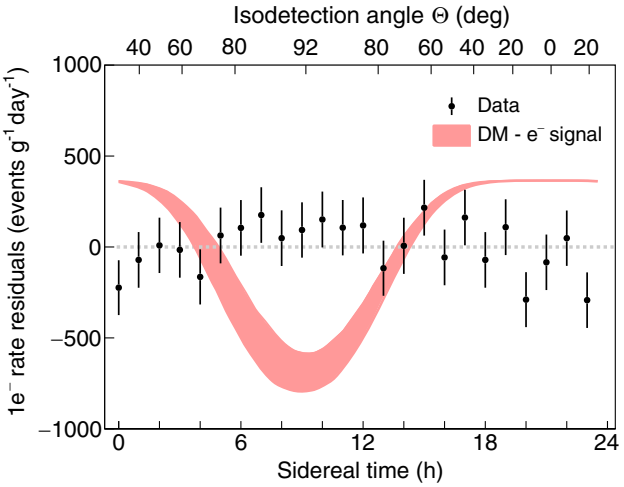

FIG. 3. U-side residual rate after the subtraction of the best-fit background-only model, binned as a function of local apparent sidereal time. As a reference, the upper x axis gives the isodetection angle $\Theta(t)$ for the first day of data taking. Each data point is obtained from the average of ~300 images. The light red band shows the expected signal (minus its time average) for a DM particle of mass 1 MeV/c^2, $\bar{\sigma}_e = 10^{-32}$ cm^2 interacting via an ultralight dark photon mediator. The signal is shown as a band because a given value of the sidereal time may correspond to a range of different Θ values, depending on the varying Earth velocity over the year. This gives rise to a time shift and amplitude change of the signal during the data-taking period.

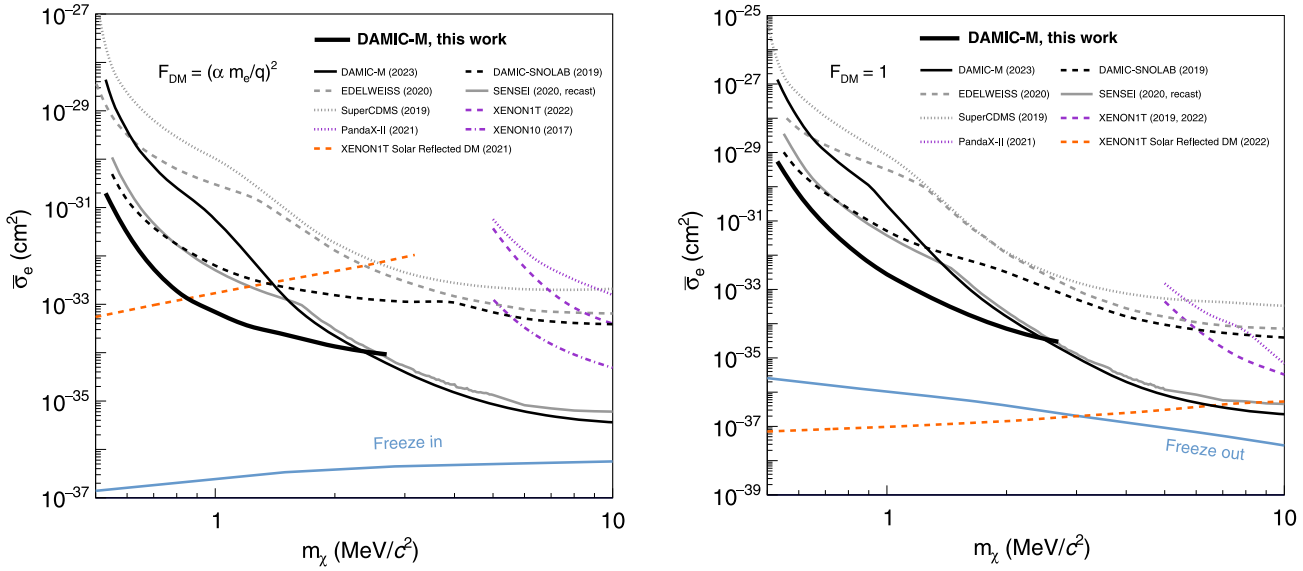

FIG. 4. DAMIC-M 90% C.L. upper limits (solid thick black) on DM-electron interactions through an ultralight (left) and heavy (right) dark photon mediator obtained from the daily modulation analysis. Also shown are previous limits from DAMIC-M [16] (solid black line) and other experiments: DAMIC-SNOLAB [13] (dashed black line); SENSEI [14,76] (solid gray line); EDELWEISS [15] (dashed gray line); SuperCDMS [12] (dotted gray line); XENON1T combined result from [77,78] (dashed violet line); PandaX-II [79] (dotted violet line); a limit obtained from XENON10 data in Ref. [80] (dash-dotted violet line); and a limit obtained from XENON1T data considering "solar reflected DM" (dashed orange line) from Ref. [81] (left) and Ref. [82] (right). Theoretical expectations assuming a DM relic abundance from freeze-in and freeze-out mechanisms are also shown in light blue line [83].

$\bar{\sigma}_e = 10^{-32}$ cm^2 (close to the current best limit on the cross section at this mass).

The fit finds no preference for a DM signal at any mass. Consequently, we derive exclusion limits using the approach of Ref. [75] and the profile likelihood ratio test statistic, $t_\sigma = -2\log\lambda(\sigma)$, where $\lambda(\sigma)$ is the profile likelihood ratio, at each DM mass. The corresponding 90% CL exclusion limits for ultralight (left) and heavy (right) mediators are shown in Fig. 4. These limits fall within the expected 95.4% sensitivity band as estimated by Monte Carlo simulations. Also shown are previous results from DAMIC-M and other direct-detection experiments. Notably, the daily modulation analysis improves up to ~2 orders of magnitude the previous DAMIC-M limits [16] obtained with the same dataset. Note that the excluded region does not extend to indefinitely large cross sections, as Earth-scattering effects eventually lead to a complete attenuation of the DM flux. For the light mediator, this upper bound occurs around $\sigma_e \approx 10^{-27}$ cm^2 over the mass range of interest. For the heavy mediator, this upper bound is at $\sigma_e \approx 10^{-27}$ cm^2 near $m_\chi = 1$ MeV/c^2, decreasing to $\sigma_e \approx 10^{-30}$ cm^2 at $m_\chi = 10$ MeV/c^2 [30]. Cross checks of the analysis are included in the Supplemental Material [48].

For DM masses ≤ 2.7 MeV/c^2 the signal is overwhelmingly composed of $1e^-$. At higher masses the $2e^-$ signal becomes relevant in establishing the exclusion limit. However, the existing cross-section constraints result in a R_2^i daily modulation amplitude that is too small to be detectable with the statistics of the current dataset. For this reason, we do not perform a full daily modulation analysis of R_2^i.

Conclusions.—This DAMIC-M search for DM particles interacting with electrons excludes unexplored regions of parameter space between 0.53 and 2.7 MeV/c^2. This is the first time that the daily modulation due to scattering of DM particles in Earth, before they reach the detector, constrains DM-electron interactions. When combined with our previous limits, DAMIC-M provides the current best constraints from searches for a nonrelativistic flux of DM particles incident on Earth, over the mass ranges [0.53, 1000] and $[0.53, 15.1]$ MeV/c^2 for ultralight and heavy mediator interactions, respectively [84]. In addition, a model-independent search for modulations with period close to 24 h demonstrates the stability of our detector, allowing for further improvements in time-dependent searches for a DM signal.

We thank the LSM for their support in the installation and operation of the detector underground. The DAMIC-M project has received funding from the European Research Council (ERC) under the European Union's Horizon 2020 research and innovation programme Grant Agreement No. 788137, and from NSF through Grant No. NSF PHY-1812654. The work at University of Chicago and University of Washington was supported through Grant No. NSF PHY-2110585. This work was supported by the Kavli Institute for Cosmological Physics at the University of Chicago through an endowment from the Kavli

Foundation. We thank the College of Arts and Sciences at University of Washington for contributing the first CCDs to the DAMIC-M project. I. F. C. A. was supported by Project No. PID2019–109829 GB-I00 funded by MCIN/AEI/10.13039/501100011033. B. J. K. acknowledges funding from the Ramón y Cajal Grant No. RYC2021-034757-I, financed by MCIN/AEI/10.13039/501100011033 and by the European Union "NextGenerationEU"/PRTR. The Centro Atómico Bariloche group is supported by ANPCyT Grant No. PICT-2018-03069. The University of Zürich was supported by the Swiss National Science Foundation. The CCD development work at Lawrence Berkeley National Laboratory MicroSystems Lab was supported in part by the Director, Office of Science, of the U.S. Department of Energy under Contract No. DE-AC02-05CH11231. We thank Teledyne DALSA Semiconductor for CCD fabrication. We acknowledge Santander Supercomputing support group at the University of Cantabria who provided access to the supercomputer Altamira at the Institute of Physics of Cantabria (IFCA-CSIC), member of the Spanish Supercomputing Network, for performing simulations.

*Now at Fermi National Accelerator Laboratory, Batavia, Illinois, USA.

[1] G. Bertone, D. Hooper, and J. Silk, Phys. Rep. **405**, 279 (2005).
[2] J. M. Gaskins, Contemp. Phys. **57**, 496 (2016).
[3] O. Buchmueller, C. Doglioni, and L. T. Wang, Nat. Phys. **13**, 217 (2017).
[4] J. Billard *et al.*, Rep. Prog. Phys. **85**, 056201 (2022).
[5] C. Boehm, P. Fayet, and J. Silk, Phys. Rev. D **69**, 101302(R) (2004).
[6] D. Hooper and K. M. Zurek, Phys. Rev. D **77**, 087302 (2008).
[7] M. Pospelov, A. Ritz, and M. B. Voloshin, Phys. Lett. B **662**, 53 (2008).
[8] X. Chu, T. Hambye, and M. H. G. Tytgat, J. Cosmol. Astropart. Phys. 05 (2012) 034.
[9] S. Knapen, T. Lin, and K. M. Zurek, Phys. Rev. D **96**, 115021 (2017).
[10] R. Essig, J. Mardon, and T. Volansky, Phys. Rev. D **85**, 076007 (2012).
[11] R. Essig, M. Fernández-Serra, J. Mardon, A. Soto, T. Volansky, and T.-T. Yu, J. High Energy Phys. 05 (2016) 046.
[12] R. Agnese *et al.* (SuperCDMS Collaboration), Phys. Rev. Lett. **121**, 051301 (2018); **122**, 069901(E) (2019).
[13] A. Aguilar-Arevalo *et al.* (DAMIC Collaboration), Phys. Rev. Lett. **123**, 181802 (2019).
[14] L. Barak *et al.* (SENSEI Collaboration), Phys. Rev. Lett. **125**, 171802 (2020).
[15] Q. Arnaud *et al.* (EDELWEISS Collaboration), Phys. Rev. Lett. **125**, 141301 (2020).
[16] I. Arnquist *et al.* (DAMIC-M Collaboration), Phys. Rev. Lett. **130**, 171003 (2023).
[17] P. Adari *et al.*, SciPost Phys. Proc. **9**, 001 (2022).
[18] C. Kouvaris and N. G. Nielsen, Phys. Rev. D **92**, 075016 (2015).
[19] P. Sikivie and S. Wick, Phys. Rev. D **66**, 023504 (2002).
[20] M. S. Alenazi and P. Gondolo, Phys. Rev. D **74**, 083518 (2006).
[21] J. I. Collar and F. T. Avignone, Phys. Lett. B **275**, 181 (1992).
[22] J. I. Collar and F. T. Avignone III, Phys. Rev. D **47**, 5238 (1993).
[23] F. Hasenbalg, D. Abriola, J. I. Collar, D. E. DiGregorio, A. O. Gattone, H. Huck, D. Tomasi, and I. Urteaga, Phys. Rev. D **55**, 7350 (1997).
[24] R. Bernabei *et al.*, Eur. Phys. J. C **74**, 2827 (2014).
[25] D. S. Akerib *et al.* (LUX Collaboration), Phys. Rev. D **98**, 062005 (2018).
[26] X. Cui *et al.* (PandaX-II Collaboration), Phys. Rev. Lett. **128**, 171801 (2022).
[27] M. Andriamirado *et al.* (PROSPECT Collaboration), Phys. Rev. D **104**, 012009 (2021).
[28] B. Holdom, Phys. Lett. **166B**, 196 (1986).
[29] P. Galison and A. Manohar, Phys. Lett. **136B**, 279 (1984).
[30] T. Emken, R. Essig, C. Kouvaris, and M. Sholapurkar, J. Cosmol. Astropart. Phys. 09 (2019) 070.
[31] C. Kouvaris and I. M. Shoemaker, Phys. Rev. D **90**, 095011 (2014).
[32] N. Ávalos *et al.*, J. Phys. Conf. Ser. **2156**, 012074 (2021).
[33] I. Arnquist *et al.*, SciPost Phys. Proc. **12**, 014 (2023).
[34] S. E. Holland, Exp. Astron. **14**, 83 (2002).
[35] S. E. Holland, D. E. Groom, N. P. Palaio, R. J. Stover, and M. Wei, IEEE Trans. Electron Devices **50**, 225 (2003).
[36] S. E. Holland, W. F. Kolbe, and C. J. Bebek, IEEE Trans. Electron Devices **56**, 2612 (2009).
[37] A. Alessandrello *et al.*, Nucl. Instrum. Methods Phys. Res., Sect. B **61**, 106 (1991).
[38] S. Agostinelli *et al.*, Nucl. Instrum. Methods Phys. Res., Sect. A **506**, 250 (2003).
[39] A. Aguilar-Arevalo *et al.* (DAMIC Collaboration), Phys. Rev. D **94**, 082006 (2016).
[40] J. Janesick, T. S. Elliott, A. Dingiziam, R. A. Bredthauer, C. E. Chandler, J. A. Westphal, J. E. Gunn, and M. M. Blouke, Proc. SPIE Int. Soc. Opt. Eng. **1242**, 223 (1990).
[41] C. E. Chandler, R. A. Bredthauer, J. R. Janesick, J. A. Westphal, and M. M. Blouke, Proc. SPIE Int. Soc. Opt. Eng. **1242**, 238 (1990).
[42] J. Tiffenberg, M. Sofo-Haro, A. Drlica-Wagner, R. Essig, Y. Guardincerri, S. Holland, T. Volansky, and T. T. Yu, Phys. Rev. Lett. **119**, 131802 (2017).
[43] D. Norcini *et al.* (DAMIC-M Collaboration), Phys. Rev. D **106**, 092001 (2022).
[44] J. R. Janesick, *Scientific Charge-Coupled Devices* (SPIE Optical Engineering Press, Bellingham, 2001).
[45] The time of each image was recorded in coordinated universal time (UTC).
[46] G. Cowan, K. Cranmer, E. Gross, and O. Vitells, Eur. Phys. J. C **71**, 1554 (2011); **73**, 2501(E) (2013).
[47] E. Gross and O. Vitells, Eur. Phys. J. C **70**, 525 (2010).
[48] See Supplemental Material at http://link.aps.org/supplemental/10.1103/PhysRevLett.132.101006 for further details on the deviation found at the modulation for $T =$ 26 h in the L side, which includes Refs. [48–54].

[49] Z. Y. Zhang *et al.* (CDEX Collaboration), Phys. Rev. Lett. **129**, 221301 (2022).
[50] P. Agnes *et al.* (DarkSide Collaboration), Phys. Rev. Lett. **130**, 101002 (2023).
[51] S. Knapen, J. Kozaczuk, and T. Lin, Phys. Rev. D **105**, 015014 (2022).
[52] S. M. Griffin, K. Inzani, T. Trickle, Z. Zhang, and K. M. Zurek, Phys. Rev. D **104**, 095015 (2021).
[53] T. Trickle, Phys. Rev. D **107**, 035035 (2023).
[54] T. Emken and C. Kouvaris, Phys. Rev. D **97**, 115047 (2018).
[55] T. Emken and C. Kouvaris, Dark matter simulation code for underground scatterings (DaMaSCUS) [Code, v1.1], https://github.com/temken/damascus; 10.5281/zenodo.3726878 (2017–2020).
[56] S. K. Lee, M. Lisanti, S. Mishra-Sharma, and B. R. Safdi, Phys. Rev. D **92**, 083517 (2015).
[57] S. M. Griffin, K. Inzani, T. Trickle, Z. Zhang, and K. M. Zurek, Phys. Rev. D **104**, 095015 (2021).
[58] A. M. Green, J. Phys. G **44**, 084001 (2017).
[59] We use the standard halo model [60] parameters with Earth's velocity fixed to its average value during the data-taking period, $v_{\mathrm{E}} = 263$ km/s.
[60] D. Baxter *et al.*, Eur. Phys. J. C **81**, 907 (2021).
[61] C. McCabe, J. Cosmol. Astropart. Phys. 02 (2014) 027.
[62] T. Emken and C. Kouvaris, J. Cosmol. Astropart. Phys. 10 (2017) 031.
[63] G. D. Starkman, A. Gould, R. Esmailzadeh, and S. K. Dimopoulos, Phys. Rev. D **41**, 3594 (1990).
[64] B. J. Kavanagh, R. Catena, and C. Kouvaris, J. Cosmol. Astropart. Phys. 01 (2017) 012.
[65] M. S. Mahdawi and G. R. Farrar, J. Cosmol. Astropart. Phys. 12 (2017) 004.
[66] D. Hooper and S. D. McDermott, Phys. Rev. D **97**, 115006 (2018).
[67] M. S. Mahdawi and G. R. Farrar, J. Cosmol. Astropart. Phys. 10 (2018) 007.
[68] B. J. Kavanagh, Phys. Rev. D **97**, 123013 (2018).
[69] B. J. Kavanagh, Verne [Code, v1.3], 10.5281/zenodo.7193430.
[70] Note that VERNE uses an alternative convention for the isodetection angle $\gamma = 180° - \Theta$.
[71] A. Lantero-Barreda and B. J. Kavanagh (to be published).
[72] Note that the isodetection angle corresponding to a given time in a sidereal day changes by several degrees during the data-taking period.
[73] K. Ramanathan and N. Kurinsky, Phys. Rev. D **102**, 063026 (2020).
[74] A. Aguilar-Arevalo *et al.* (DAMIC Collaboration), Phys. Rev. D **105**, 062003 (2022).
[75] G. Cowan, K. Cranmer, E. Gross, and O. Vitells, Eur. Phys. J. C **71**, 1554 (2011).
[76] The recast limit, provided by the SENSEI Collaboration, uses the same halo parameters and charge yield model of Ref. [16] for proper comparison.
[77] E. Aprile *et al.* (XENON Collaboration), Phys. Rev. Lett. **123**, 251801 (2019).
[78] E. Aprile *et al.* (XENON Collaboration), Phys. Rev. D **106**, 022001 (2022).
[79] C. Cheng *et al.* (PandaX-II Collaboration), Phys. Rev. Lett. **126**, 211803 (2021).
[80] R. Essig, T. Volansky, and T.-T. Yu, Phys. Rev. D **96**, 043017 (2017).
[81] H. An, H. Nie, M. Pospelov, J. Pradler, and A. Ritz, Phys. Rev. D **104**, 103026 (2021).
[82] T. Emken, Phys. Rev. D **105**, 063020 (2022).
[83] M. Battaglieri *et al.*, arXiv:1707.04591.
[84] Complementary searches for semirelativistic DM fluxes from Solar reflection [81,82] and cosmological [85,86] and stellar evolution constraints [87,88] also place limits in this mass range.
[85] G. Krnjaic and S. D. McDermott, Phys. Rev. D **101**, 123022 (2020).
[86] C. Giovanetti, M. Lisanti, H. Liu, and J. T. Ruderman, Phys. Rev. Lett. **129**, 021302 (2022).
[87] S. Davidson, S. Hannestad, and G. Raffelt, J. High Energy Phys. 05 (2000) 003.
[88] J. H. Chang, R. Essig, and S. D. McDermott, J. High Energy Phys. 09 (2018) 051.